RSC Advances

ROYAL SOCIETY OF CHEMISTRY

www.rsc.org/advances

Synthesis of g-C_3N_4 prepared at different temperatures for superior visible/UV photocatalytic performance and photoelectrochemical sensing of MB solution

Zhao Mo, Xiaojie She, Yeping Li, Liang Liu, Liying Huang, Zhigang Chen, Qi Zhang, Hui Xu*, Huaming Li*

School of Chemistry and Chemical Engineering, Institute for Energy Research, Jiangsu University,

Zhenjiang 212013, P. R. China. E-mail: xh@ujs.edu.cn, lihm@ujs.edu.cn

Fax: +86-511-88791708; Tel: +86-511-88791800

Abstract: In this paper, a simple and convenient preparation method was utilized to study for the optimum calcination temperature of graphitic carbon nitride (g-C_3N_4). The g-C_3N_4 prepared at different temperatures was characterized by X-ray diffraction (XRD), UV-vis diffuse reflectance spectroscopy (DRS) and so on. The results demonstrated that g-C_3N_4 could not be formed fully until the calcination temperature was higher than 500°C. From DRS and PL spectras, a red shift of absorption peaks with increasing calcination temperatures was both found. This could enhance the visible light absorption, and then the photocatalytic activity would be improved. The photocatalytic activity was evaluated via the photodegradation of methylene blue (MB) and 4-chlorophenol (4-CP), respectively. Moreover, due to the gradual decrement trend of photocurrent intensity with addition of MB, g-C_3N_4 prepared at 650°C can be used as a photoelectrochemical sensor to detect the existence of MB and estimate the concentration of MB. Hence g-C_3N_4 will become a promising candidate for photoelectrochemical applications.

1. Introduction

The increasing threats of environmental issues and energy shortage have hindered the development and survival of human society, numerous scientists and researchers are seeking green technologies to solve these problems.[1] Because of several advantages such as clean, safe, economic and renewable properties, semiconductor photocatalytic technology has become a promising way over the past decade,[2,3] which has been applied in many fields, such as degradation of organic pollutants,[4] hydrogen evolution,[5-7] energy storage,[8,9] electronics,[10] supercapacitors[11] and CO_2 photocatalytic reduction to hydrocarbon compounds.[12,13]

The origin of semiconductor photocatalytic technology begins with the work of TiO_2 electrodes for hydrogen evolution reaction.[14] From then on, more and more researchers have devoted themselves to designing novel and highly efficient photocatalysts. As a promising "metal-free" and visible lighted photocatalyst, carbon nitride has several allotropes, the graphitic phase is the most stable phase under ambient conditions.[15] The g-C_3N_4 was first synthesized by Berzelius and named "melon" by Liebig in 1834, it is a polyconjugated semiconductor composed of carbon and nitrogen atoms and it possesses a layered graphite-like structure.[16] g-C_3N_4 is not only economic and environmental friendly, but also has unbeatable physicochemical properties of high chemical stability, thermal stability, photoelectrochemical property, inoxidizability, biological compatibility and waterproofness, which make g-C_3N_4 become valuable materials for photocatalysis-driven applications and has attracted a lot of attention from researchers.[17] Unlike TiO_2, which is only a ultraviolet lighted photocatalyst, g-C_3N_4 is active in the visible region, which is due to its band gap energy of about 2.7 eV with suitable CB and VB positions (-1.1 eV and +1.6 eV, respectively).[18] The synthesis strategies of g-C_3N_4 have been summarized by Thomas,[19] such as thermal condensation, thermal nitridation, PVD (physical vapor deposition), CVD (chemical vapor deposition), solid state reaction and solvothermal method. It is worth noting that thermal condensation, as a simple and feasible method, has been the main method of synthesizing g-C_3N_4.[1] The precursors of preparing g-C_3N_4 by thermal condensation are usually nitrogen-rich materials, such as urea, cyanamide, dicyandiamide, melamine and thiourea.[20] Just because of superior physicochemical properties and simple synthesis method, g-C_3N_4 has been applied in many photocatalytic areas, such as photocatalytic hydrogen evolution, photocatalytic CO_2 reduction, photocatalytic degradation of pollutants, photocatalytic organic syntheses and photocatalytic disinfection.[21] However, due to the hindered marginal absorption of visible light and grain boundary effects, the efficiency of g-C_3N_4 in visible light is rather low.[22] Therefore, it is very necessary to extend light absorption of g-C_3N_4. At the same time, the small surface area, the low quantum efficiency and low separation efficiency but high recombination rate of photogenerated electron-hole pairs still limit the development of g-C_3N_4.[23,24] Many modification endeavors have been used to modify the electronic structures of g-C_3N_4 and enhance the photocatalytic performance of g-C_3N_4, such as noble metal deposition (Ag,[25] Au,[26] Pt,[27] AuPd[28]); nonmetal doping (N,[29] P,[30] S[31]); metallic oxide compositing (CeO_2,[32]

WO_3,[33] Fe_2O_3,[34] Co_3O_4[35]); dye sensitization[36], designing novel nanostructures.[37] and designing an appropriate g-C_3N_4 textural structure.[17] Except the above strategies, many literatures also reported the synthesis conditions of materials may affect the photocatalytic performance of g-C_3N_4, traditional synthesis conditions mainly included the following, such as temperature,[38,39] synthesis medium,[40] atmosphere[41] and pressure.[42] The control of calcining temperature is easy relatively, which not only influences the surface microstructures of the photocatalysts, but also affects the photocatalytic activity. Therefore, the modification of g-C_3N_4 is very efficient to improve the optical absorption and photocatalytic performance.

As a promising and simple analytical technique, photoelectrochemistry uses photocurrent as a detection signal, which has been drawn more attention.[43] Generally, the sensor is a molecular receptor, which has changeable optical properties because of binding specific guests. Some photoelectrochemical materials (TiO_2, SnO_2, CdS, CdSe and g-C_3N_4) have been used as sensors.[21] The g-C_3N_4 as a receptor can perform high sensitivity for photoelectrochemical detection. Some researches have proved that g-C_3N_4 exhibits excellent sensitivity for the detection of trace amounts of Cu^{2+}.[33,44]

In this work, melamine was chosen as the precursor, g-C_3N_4 was prepared by thermal condensation under different temperatures (450, 500, 550, 600, and 650°C). The photocatalytic activity was evaluated by photodegrading MB and 4-CP. Thus the influence of calcination temperature was obtained and the possible visible/UV photocatalytic mechanisms were discussed. Finally, it is worth noting that g-C_3N_4 can not only be used as a photocatalyst to degrade MB and 4-CP, but also can be a photoelectrochemical sensor to detect the existence and concentration of MB solution. The possible mechanism for the photoelectrochemical detection of MB was also discussed.

2. Experimental

2.1 Preparation of g-C_3N_4

The g-C_3N_4 was prepared by directly heating melamine in a muffle furnace. 2 g melamine was put into a alumina crucible with a cover and calcined at 450, 500, 550, 600, and 650°C with a heating rate of 2°C/min, then kept for 2 h at this temperature. Finally, the coarse g-C_3N_4 was grinded into the powder before further characterization. The Schematic illustration of g-C_3N_4 prepared at different temperatures was shown in Fig. S1.

2.2 Characterization of g-C_3N_4 prepared at different temperatures

The as-prepared g-C_3N_4 was analyzed by X-ray diffraction (XRD) by Bruker D8 diffractometer with Cu Kα radiation (λ=1.5418 Å) in the range of 2θ=10-80°. The Fourier transform infrared spectra (FT-IR) of the samples were recorded using Nicolet Nexus 470 spectrometer. The morphology and structure of the samples were investigated with scanning electron microscope (SEM) and transmission electron microscopy (TEM). The SEM images were taken on a field-emission microscope by a JEOL JSM-7001F. The chemical composition of the samples was determined by an energy-dispersive X-ray spectroscope (EDS) operated at an acceleration voltage of 10 kV. The transmission electron microscopy (TEM) images were collected with a JEOL-JEM-2010 (JEOL, Japan) operated at 200 kV. The Brunauer-Emmett-Teller (BET) specific surface area of samples was recorded by using a Micromeritics TriStar II 3020 nitrogen adsorption apparatus (USA). All of the samples were degassed at 180°C before measurement. The BET surface area was determined by a multipoint BET method using the adsorption data in the relative pressure (P/P_0) range of 0.05-0.25. Elemental compositions were detected by X-ray photoelectron spectroscopy (XPS) analysis which was performed on an ESCALab MKII X-ray photo-electron spectrometer using the Mg Kα radiation. Ultraviolet visible (UV-vis) diffuse reflectance spectrums (DRS) of the samples were measured by using a UV-vis spectrophotometer (Shimadzu UV-2450, Japan) in the range of 200 to 800 nm. $BaSO_4$ was used as the reflectance standard material. The photoluminescence (PL) spectra of the samples were obtained by a QuantaMaster & TimeMaster Spectrofluorometer with an excitation wavelength at 325 nm. X-band ESR spectra were recorded at ambient temperature on a JES FA200 spectrometer. The settings for the ESR spectrometer were as follows: center field, 336.496 mT; sweep width, 5 mT; microwave frequency, 9.5 GHz; modulation frequency, 100 kHz; power, 0.998 mW.

2.3 Photoelechemical measurements

The photocurrents were measured with an electrochemical analyzer (CHI660B, Chen Hua Instruments, Shanghai, China) in a standard three-electrode configuration with a platinum wire as the counter electrode, Ag/AgCl (in saturated KCl) as a reference electrode, and Na_2SO_4 (0.1 M) aqueous solution as the electrolyte. A 500W Xe arc lamp was utilized as a light source. 5 mg sample powder was dispersed ultrasonically in 1 mL of mixed solution (0.5 mL ethanol and 0.5 mL ethanediol), and 20 μL of the resulting colloidal dispersion (5 mg/mL) was drop-cast onto a piece of

ITO with a fixed area of 0.5 cm^2, and dried under an infrared lamp to form the sample-modified ITO electrode. All the photocurrent measurements were performed at a constant potential of -0.2 V (*vs.* SCE).

2.4 Photocatalytic activity

The photocatalytic activity of the prepared samples was evaluated by the photocatalytic degradation of MB solution under visible/UV light irradiation and 4-CP solution under UV light irradiation. A 300 W Xe lamp as the light source was set in the middle of the photocatalytic reactor. To provide the visible light for the photocatalytic reaction, a 400 nm cutoff filter was set beside the lamp. Moreover, the 100 ml quartz glass beaker which contained the photocatalyst and MB solution was set next to the cutoff filter and the distance between the center of the beaker and the lamp was about 10 cm. They were all at the same height and the light could irradiate the beaker evenly. In all the photocatalytic experiments, the lamp and the quartz glass beaker were set at the same place. So the light intensity was fixed. In each experiment, 0.0250 g photocatalysts were dispersed into the 50 mL MB solution (10 mg/L) in a Pyrex potocatalytic reactor respectively. The reaction mixture was continuously aerated by a pump to provide O_2. Prior to irradiation the suspensions were magnetically stirred for 30 min in the dark to ensure that the MB could reach the absorption-desorption equilibrium on the photocatalyst surface. Furthermore, all experiments were performed at 30°C under constant stirring. At defined time irradiation intervals, 3 mL solution suspension was withdrawn and centrifuged (13000 rpm, 3 min) to separate the photocatalyst, the filtrates of MB analyzed with a UV-vis spectrophotometer (UV-2450, Shimadzu) at the maximal absorption wavelength of MB whose characteristic absorption peak was chosen to be 664 nm.

A medium pressure 250 W mercury vapor lamp was used as the UV source. In each experiment, 0.0250 g photocatalysts were dispersed into the 50 mL 4-CP solution (10 mg/L) in a Pyrex potocatalytic reactor respectively. The concentration of 4-CP was determined by a HPLC (Waters 1525) system, all substances were detected by a UV detector at 280 nm, the eluent consisted of a ternary mixture of water, methanol and acetonitrile (40:50:10 by volume), the flow rate was 1mL min^{-1}. The other experimental conditions were the same as the photocatalytic degradation of MB.

The photocatalytic degradation efficiency (*E*) was obtained by the following formula:

$$E = (1 - \frac{C}{C_0}) \times 100\% = (1 - \frac{A}{A_0}) \times 100\%$$

Where C is the concentration of the solution at reaction time t, C_0 is the adsorption/desorption equilibrium concentration at reaction time t_0, A and A_0 are the corresponding values.

3. Results and discussion

3.1 Enhancement of photocatalytic activity

The photocatalytic activity of g-C_3N_4 prepared at different temperatures was tested via the photodegradation of MB under visible light irradiation, as shown in Fig. 1a. The adsorption test was pre-conducted in dark for 30 min and then degradation proceeded at t=0. The adsorption test results showed that the absorption-desorption equilibrium has been reached, so the adsorption of MB over each sample could be neglected under visible light irradiation. The adsorption efficiencies of g-C_3N_4 prepared at 500, 550, 600°C and 650°C were about 9.21%, 11.56%, 15.77% and 35.25% for MB, respectively. It could be seen clearly that, g-C_3N_4 prepared at 650°C exhibited highest adsorptive ability and the adsorption efficiency of g-C_3N_4 increased with increasing temperatures, these were consistent well with their surface areas. It was found that g-C_3N_4 prepared at 650°C exhibited the highest photocatalytic activity, the photocatalytic degradation efficiency of MB was up to about 82.50% after 3.5 h irradiation. The photocatalytic degradation efficiency of g-C_3N_4 prepared at 500, 550 and 600°C were about 18.92%, 26.41%, 36.70% after 3.5 h irradiation, respectively. At the same time, the photocatalytic degradaion of MB under UV light irradiation was done and the results were shown in Fig. 1b. It can be seen clearly that, the photocatalytic degradation efficiency of g-C_3N_4 prepared at 500, 550 600 and 650°C were about 54.30%, 55.75%, 64.06% and 90.07% after 140 min UV light irradiation respectively. The g-C_3N_4 prepared at 650°C exhibited the highest photocatalytic activity under UV light irradiation, which agreed with the photocatalytic degradaion of MB under visible light irradiation. Obviously, it was interesting that, from the results of photocatalytic degrading MB under visible and UV light irradiation, the photocatalytic activity of g-C_3N_4 increased with increasing temperatures, indicating that the calcination temperature of g-C_3N_4 affected photocatalytic activity, the higher calcination temperature may enhance the photocatalytic degradation efficiency. Compared with g-C_3N_4 prepared at 500, 550 and 600°C, the photocatalytic

degradation efficiency of g-C_3N_4 prepared at 650°C has been greatly improved.

In the meantime, the photocatalytic activity of g-C_3N_4 prepared at different temperatures was further studied by 4-chlorophenol (4-CP) as model colorless organic pollutant, which was shown in Fig. S2a. The photocatalytic degradation efficiency of g-C_3N_4 prepared at 500, 550, 600 and 650°C was about 79.18%, 84.90%, 89.81% and 66.62% respectively. The results indicated that g-C_3N_4 prepared at different temperatures also showed a high photo-catalytic activity in degrading 4-CP.

3.2 Kinetics

The kinetics of MB photodecomposition on the catalyst surface can be described by the pseudo-first-order reaction model

$$ln(C_0/C) = kt$$

where k was the reaction rate constant, C_0 was the concentration of MB when the absorption-desorption equilibrium has been reached, and C was the actual concentration of MB at reaction time t. Fig. 2 presented the linear relationship between $ln(C_0/C)$ and the reaction time for MB, g-C_3N_4 prepared at 650 °C exhibited higher photocatalytic degradation rate than g-C_3N_4 prepared at 500, 550 and 600°C. The reaction rate constant (k) and relative coefficient (R^2) were summarized in *Table S1*. Reaction rate constant k was the slope of the linear relationship of the natural logarithm of the ratio between the initial concentration of MB and the actual concentration versus the corresponding reaction time. For g-C_3N_4 prepared at 500, 550, 600 and 650°C, the corresponding reaction rate constants (k) were calculated to be 0.0315 h^{-1}, 0.0545 h^{-1}, 0.0765 h^{-1} and 0.3619 h^{-1}, respectively. The largest reaction rate constant k of g-C_3N_4 prepared at 650°C was 0.3619 h^{-1}, which was 11.5 times higher than that of g-C_3N_4 prepared at 500°C. Moreover, the reaction rate constant k of g-C_3N_4 prepared at 550 and 600°C was 2.4 and 1.7 times as high as that of g-C_3N_4 prepared at 500°C. The increased reaction rate could be because of greater absorption of the incident visible light, thereby generating more photo-generated electrons to make charge separation more efficient, after that the photocatalytic activity enhanced.

Moreover, the stability of the photocatalyst was also an important factor to influence its practical application. As shown in Fig. 3, the photocatalytic activity of g-C_3N_4 prepared at 650°C only reduced a little after four cycles, this could be due to the loss of g-C_3N_4 during the test period. The results indicated that g-C_3N_4 prepared at 650°C had a satisfying stability.

3.3 Photoelectrochemical detection of MB

Fig. 4a depicted the typical time-based photocurrent response of the photoelectrochemical sensor in the presence of different concentrations of MB. It could be seen that the rise and fall of the photocurrent conformed well to the irradiation being switched on and off. The photocurrent response of the electrode modified by g-C_3N_4 prepared at 650°C decreased gradually for every 5 μL increase of MB. Fig. 4b showed the linear calibration plots between the photocurrent response and the concentrations of MB. The linear regression equation was y = -0.0084x + 1.1328 with a correlation coefficient (R^2) of 0.9951.

3.4 Structure and morphology characterization of g-C_3N_4 prepared at different temperatures

XRD patterns were used to identify the crystal structure of g-C_3N_4 prepared at different temperatures, which were shown in Fig. 5. The XRD patterns of g-C_3N_4 prepared at 500, 550, 600, and 650°C showed two major diffraction peaks which occurred at around 13.1° and 27.3°, and no diffraction peaks of other impurity phase were detected in all the samples. The strong peak at around 27.3° could be indexed as (200), which was due to interplanar stacking of aromatic systems. The weak one at 13.1° is corresponding to (100) plane, which put down to an in-planar structural packing motif. These two characteristic diffraction peaks were consistent with the g-C_3N_4 reported before.[33] However, in the XRD pattern, it was found that the characteristic peaks of sample synthesized at 450°C were different from other samples, which belonged to melem derivatives.[45] This phenomenon may be put down to the low polycondensation intermediate of melamine.[18] The XRD patterns indicated that when the calcination temperature was lower than 500°C, the crystal structure was different from g-C_3N_4, this meant that the sample synthesized at 450°C was not g-C_3N_4. Then, when the calcination temperature was higher than 500°C, the samples fully formed into g-C_3N_4. In addition, as shown in Fig S3, when the calcination temperature reached 700°C, it was empty in the alumina crucible after calcination, which indicated that g-C_3N_4 could be completely decomposed.

The chemical structure of g-C_3N_4 prepared at different temperatures was further investigated by FT-IR spectroscopy, as shown in Fig. 6. No obvious difference can be observed in the spectra of g-C_3N_4 synthesized at 500, 550, 600, and 650°C. All IR bands resembled the absorption bands of the pure g-C_3N_4 reported before.[4] Comparing with g-C_3N_4 synthesized at 500, 550, 600, and 650°C, the absorption

peaks of g-C_3N_4 (450°C) between 1000 and 1750 cm^{-1} were broader, This phenomenon also meant that there were intermediate products such as ammelide in the sample. Thus the sample synthesized at 450°C was not g-C_3N_4, which was consistent with the previous XRD result shown in Fig. 5. The strong peaks at 1640, 1564, 1412, 1326 and 1241 cm^{-1} were attributed to the typical stretching modes of C=N and C-N heterocycles.[47] In addition, The sharp band at 812 cm^{-1} was observed,[46, 48] which can be assigned to the characteristic breathing mode of the s-triazine units. The broad bands between 3600 cm^{-1} and 3000 cm^{-1} were assigned to N-H stretching and a small number of adsorbed H_2O.[49] All the characteristic peaks of g-C_3N_4 can be found from FT-IR spectra of g-C_3N_4 synthesized at 500, 550, 600, and 650°C, indicating that only when the calcination temperature is higher than 500°C, the samples fully formed into g-C_3N_4.

Fig. 7 showed the SEM and TEM images of g-C_3N_4 prepared at different temperatures, which investigated the microstructure of g-C_3N_4 prepared at different temperatures. The Fig. 7a showed the morphology of g-C_3N_4 prepared at 500°C was lumpy. It can be clearly seen from Fig. 7b to Fig. 7d, with the temperature increasing, g-C_3N_4 became more and more slagking gradually, this can effectively increase the surface area of g-C_3N_4. As we known the enlarged surface area could provide more active sites and absorption sites to adsorb reactants. Typical TEM images of g-C_3N_4 prepared at different temperatures could be seen from Fig. 7e to Fig. 7h, the structure of g-C_3N_4 became much thinner and fluffier. It was worth noting that a few pores appeared on the surface of g-C_3N_4 prepared at 600°C and when the calcination temperatures rose to 650°C, many pores started to fuse, which may increase the surface area of g-C_3N_4 greatly. The high-magnification TEM image of g-C_3N_4 prepared at 650°C was shown in Fig 7i, which showed g-C_3N_4 prepared at 650°C was almost transparent, this was due to its thin structure. The results indicated that g-C_3N_4 prepared at 650°C was fluffy.[51]

The chemical composition of g-C_3N_4 synthesized at 650°C was confirmed by EDS, Which was shown in Fig. 7j. The peaks of C, N were observed and no other impurity peak was found, except the peak of Si (this was attributed to the silicon wafers), the result indicated that the sample synthesized at 650°C was still g-C_3N_4.

In order to determine whether the specific surface area of g-C_3N_4 increased with varying calcination temperature, the nitrogen adsorption-desorption isotherms were shown in Fig. S4. The BET specific surface areas were 7.1 $m^2 g^{-1}$, 8.6 $m^2 g^{-1}$, 11.7 m^2

g^{-1}, and 46.8 $m^2 g^{-1}$ for g-C_3N_4 prepared at 500, 550, 600, and 650°C, respectively. The BET specific surface area of g-C_3N_4 prepared at 650°C was about 6.6 times of g-C_3N_4 prepared at 500°C. These results further demonstrated that the surface area of g-C_3N_4 has been improved greatly with the temperature increasing, which was also in accordance with the observed morphology in the SEM and TEM images. The enlarged surface area can offer more reactive sites and adsorb more pollutants. Thus, the photocatalytic performance can be improved.

The XPS spectra were measured to determine the chemical composition and chemical states of g-C_3N_4 prepared at different temperatures, as shown in Fig. 8. The survey XPS spectra of g-C_3N_4 prepared at different temperatures showed similar features. In addition, C, N and a small amount of O peaks (which is usually ascribed to the adsorbed water) can be found in all samples and no peaks of other elements are observed, indicating that all the samples keep the same chemical composition and chemical states. As shown in Fig. 8b, the high-resolution C 1s spectra of g-C_3N_4 prepared at different temperatures showed similar features, then C 1s could be further separated into two peaks at about ~288.26 and ~284.81 eV, which were related to the N-C-N coordination and carbon contamination, respectively.[50] Fig. 8c showed the high-resolution N 1s spectra of g-C_3N_4 prepared at different temperatures, the positions and intensities corresponding to main peaks of all the samples were the same. It could be found that N 1s could be deconvoluted into three peaks at about ~398.69 eV, ~399.99 and ~401.35 eV, respectively. The peak at about ~398.69 eV can be ascribed to the aromatic N bonded to two carbon atoms (C=N-C).[2] Two other peaks at about ~399.99 and ~401.35 eV were assigned to the tertiary N bonded to carbon atoms (C-N(-C)-C) and the amino function group carrying a hydrogen (C-N-H).[51] Thus, According to the above XPS analysis, no obvious binding energy shift of g-C_3N_4 prepared at different temperatures has been found, indicating that all the g-C_3N_4 prepared at different temperatures were at the same chemical states.

3.5 Optoelectronic properties

The optical property played an important role in the photocatalytic activity, so the DRS spectra of g-C_3N_4 prepared at different temperatures were investigated, as shown in Fig. 9a. It can be seen that as the color of g-C_3N_4 prepared at different temperatures shifted from light yellow to darkorange, there was an obvious redshift of the range 470-570 nm in the absorption band edge, which indicated increasing temperatures enhanced the absorption in the visible light region. The enhanced light

absorption of g-C_3N_4 prepared at 650°C contributed to producing more electron-hole pairs under the visible light irradiation. The redshift may be caused by the increase of the polymerization degree and the π-plane conjugation degree. This could enhance the visible light absorption effectively. From Fig. 9b, it can be seen that the band gap energy of g-C_3N_4 prepared at 500, 550, 600°C and 650°C was estimated to be about 2.83 eV, 2.78 eV, 2.71 eV and 2.74 eV, respectively. This indicated that the band of g-C_3N_4 got narrower with the calcination temperature increased, which could improve the photocatalytic activity of g-C_3N_4. Therefore the g-C_3N_4 prepared at 600°C and 650°C had a higher efficiency for absorbing visible light. However, the structure of g-C_3N_4 prepared at 650°C was fluffier, so compared with g-C_3N_4 prepared at 600°C, g-C_3N_4 prepared at 650°C stayed slightly blueshifted, this may be due to the quantum confinement effect.

The separation efficiency of photogenerated electrons and holes was investigated by photoluminescence spectra analysis, Fig. S5 showed the PL spectra of g-C_3N_4 prepared at different temperatures. The position of the emission peak of g-C_3N_4 prepared at different temperatures was located at 456, 466, 483 and 491 nm. It can be clearly found that, the center of PL showed a slightly red shift with the temperature rising constantly. At the same time, The PL intensities of g-C_3N_4 decreased with increasing temperatures from 500°C to 650°C. This indicated that g-C_3N_4 prepared at 650°C could have a lowest recombination rate of photoinduced electron and hole. Therefore, increasing temperatures was conducive to the separation of photoinduced electron and electron hole in g-C_3N_4, which exhibited that higher temperature can bring about higher photoactivity.

To further understand the separation and transfer of photoinduced electron-hole, the transient photocurrent responses of g-C_3N_4 prepared at different temperatures were monitored by using intermittent on-off irradiation cycles, as shown in Fig. 11. When the light was on, the photocurrent intensity increased to a constant value. Then come back to a constant value until the light was turned off. The photocurrents of the samples presented a good reproducibility and stable. The photocurrent responses of g-C_3N_4 increased with increasing temperatures (from 450°C to 650°C). This indicated that, as the synthesized temperatures rose, the separation and transfer of photoinduced electron-hole were more and more efficient. The photocurrent of g-C_3N_4 prepared at 650°C showed the highest efficient, which was conducive to photocatalytic activity.

Besides that, the photogenerated charge separation process can also be investigated by electrochemical impedance spectroscopy (EIS). The EIS Nyquist plots of g-C_3N_4 prepared at different temperatures in dark were shown in Fig. S6. The smaller arc radius meant a higher efficiency of separation and charge transfer. Obviously, the arc radius of g-C_3N_4 prepared at 650°C was the smallest, so g-C_3N_4 prepared at 650°C presented the fastest charge transfer rate, this phenomenon was consistent with the result of photocurrent responses.

3.6 Possible photocatalytic mechanism and detection mechanism

The efficiency of separation and transfer of photoinduced electron-hole was known as the key factor to improve the photocatalytic activity.[15] Therefore, the higher calcination temperature may enhance the efficiency of separation and transfer of photoinduced electron-hole of g-C_3N_4. Thus the photocatalytic activity of g-C_3N_4 was improved. The potential positions of the conduction band (CB) and valence band (VB) of g-C_3N_4 may affect the efficiency of separation and transfer of photoinduced electron-hole. The VB of g-C_3N_4 prepared at different temperatures were examined by the valence band X-ray photoelectron spectroscopy (VB XPS), this method has been widely used in some scientific researches,[52,53] which was shown in Fig 10a. It can be seen clearly that, the values of E_{VB} about g-C_3N_4 prepared at 500, 550, 600 and 650°C were revealed to be about 1.77 eV, 1.74 eV, 1.69 eV and 1.81 eV, respectively. E_g was the band gap energy of the semiconductor, in Fig. 9b, E_g of g-C_3N_4 prepared at 500, 550, 600 and 650°C were estimated to be about 2.83 eV, 2.78 eV, 2.71 eV and 2.74 eV, respectively. Due to $E_{CB} = E_{VB} - E_g$, the values of E_{CB} was counted to be about -1.06 eV, -1.04 eV, -1.02 eV and -0.93 eV, respectively. According to the potentials of the CB and VB edges, the schematic illustration of the band structures of g-C_3N_4 prepared at different temperatures was shown in Fig. 10b. It could be found that the conduction band and valence band potentials of g-C_3N_4 became more negative with the calcination temperature increased except g-C_3N_4 prepared at 650°C. But the conduction band and valence band potentials of g-C_3N_4 prepared at 650°C were also more negative than g-C_3N_4 prepared at 550°C and 500°C. The more negative conduction band and valence band potentials enhanced the effective separation and transfer of photoinduced electron-hole, so the MB and 4-CP could be degraded more efficient with the calcination temperature increased.

To further study the photocatalytic mechanism, the main active oxygen species which contributed to the photocatalytic activity were investigated by the ESR

measurements. As shown in Fig. 12a, no obvious ESR signal was found in the dark. From Fig. 12b, the characteristic peaks of superoxide radicals (O_2•$^-$) were observed under visible light irradiation, but there was no characteristic peaks of hydroxyl radicals (OH•). It could be seen clearly in Fig. 12c, it was similar to Fig. 12b and the ESR signal intensity of superoxide radicals (O_2•$^-$) became stronger under UV light irradiation than which under visible light irradiation. It could be understood that, UV-light could release more energy than visible light. To sum up in conclusion, O_2•$^-$ radicals are the active oxygen species in photodegradation of pollutants. In addition, as everyone knows, holes (h^+) could oxidize organic pollutants directly. Thus the synergistic effect of O_2•$^-$ radicals and holes (h^+) photodegradated organic pollutants in the photocatalytic reaction system. Based on the ESR measurements, the photocatalytic mechanism of g-C_3N_4 in the degradation of MB under the visible light irradiation was shown in Fig. 13. When the visible or UV light irradiated, g-C_3N_4 could produce photo-generated electrons and holes, the electrons of g-C_3N_4 jump into the conduction band, and the electrons combined with O_2 to generate superoxide radicals (O_2•$^-$), then superoxide radicals (O_2•$^-$) could photodegradate organic pollutants. In addition, the photoinduced holes could participate in the photocatalytic oxidation reactions directly.

In the present experiments of photocatalytic degrading MB under visible and UV light irradiation, the g-C_3N_4 prepared at 650°C showed the highest photocatalytic activity. The enhanced photocatalytic activity could be attributed to the synergistic effect. Firstly, high specific surface area can provide more active sites and absorption sites, which may play an important role in the photocatalytic activity. Secondly, the enhanced efficiency of separation and transfer of photoinduced electron-hole was also good for the photocatalytic activity. Finally, the enhanced visible-light absorption may play a very important role in the photocatalytic degradation of MB under visible light irradiation, which was proved by the DRS spectra.

The possible photoelectrochemical mechanism for detection of MB was discussed in Fig. 14. When the visible light irradiated the surface of the ITO/g-C_3N_4 electrode, the g-C_3N_4 prepared at 650°C was excited and underwent charge-separation to generate electrons (e^-) and holes (h^+). First, photo-generated electron transfered to the ITO electrode, and then transfered to the Pt reference electrode and transferred to g-C_3N_4 and recombine with holes, forming a cycle. When MB was added into solution, MB can be adsorbed by g-C_3N_4. This phenomenon can be observed, when

the concentration of MB in the system of the electrode was increased, as shown in Fig. S7. Thus, the surface of g-C_3N_4 would adsorb more and more MB with increase of MB gradually, this would inhibit the excitation of g-C_3N_4. Therefore, the separation rate of photoinduced electron-hole was slowed down, which could lead to decrease of the photocurrent response. Based on the gradual decreased tendency of photocurrent response, the g-C_3N_4 prepared at 650°C could be used as a photoelectrochemical sensor for detecting the concentration of MB.

4. Conclusions

In summary, g-C_3N_4 prepared at different temperatures was fabricated by a simple procedure and lower-priced precursor (melamine). The g-C_3N_4 showed a better photocatalytic activity for MB photodegradation with the calcination temperature increasing and g-C_3N_4 prepared at 650°C exhibited the highest photocatalytic activity, at the same time g-C_3N_4 prepared at 650°C had an extraordinary stability after four cycles. Moreover, the photocatalyst can also photodegrade colorless organic pollutant under UV-light irradiation. The proposed photoelectrochemical sensor shows high sensitivity about the existence and concentration of MB, which opens up a new perspective for the photoelectrochemical application. Further research analysis revealed that, the enhanced photocatalytic activity and sensitive photoelectrochemical detection may come from (a) the enhanced visible-light absorption (the main reason), (b) the much fluffier structure with higher calcination temperature, (c) more reactive sites provided by enlarged surface area, (d) the extraordinary efficiency of the separation and transfer of photoinduced electron-hole.

Acknowledgements

The authors genuinely appreciate the financial support of this work from the National Nature Science Foundation of China. The authors genuinely appreciate the financial support of this work by the National Nature Science Foundation of China (21476097, 21476098，21407065 and 21406094), the Natural Science Foundation of Jiangsu Province (BK20131207 and BK2012717, BK20140533).

References

1. S. W. Cao, J. X. Low, J. G. Yu and M. Jaroniec, *Adv. Mater.*, 2015, **27**, 2150-2176.
2. H. Xu, Y. X. Song, Y. H. Song, J. X. Zhu, T. T. Zhu, C. B. Liu, D. X. Zhao, Q. Zhang and H. M. Li, *RSC Adv.*, 2014, **4**, 34539-24547.
3. M. Bowker, *Green Chem.*, 2011, **13**, 2235-2246.
4. Y. J. Cui, Z. X. Ding, P. Liu, M. Antonietti, X. Z. Fu and X. C. Wang, *Phys. Chem. Chem. Phys.*, 2012, **14**, 1455-1462.
5. S. Trasatti, *J. Electroanal. Chem.*, 1972, **39**, 163-184.
6. Z. L. Wang, J. M. Yan, Y. Ping, H. L. Wang, W. T. Zheng and Q. Jiang, *Angew. Chem. Int. Ed.*, 2013, **52**, 4406-4409.
7. X. B. Chen, S. H. Shen, L. J. Guo, S and S. Mao, *Chem. Rev.*, 2010, **110**, 6503-6570.
8. Y. W. Zhu, S. Murali, M. D. Stoller, K. J. Ganesh, W. W. Cai, P. J. Ferreira, A. Pirkle, R. M. Wallace, K. A. Cychosz, M. Thommes, D. Su, E. A. Stach and R. S. Ruoff, *Sci.*, 2011, **332**, 1537-1541.
9. C. H. Xu, B. H. Xu, Y. Gu, Z. Q. Xiong, J. Sun and X. S. Zhao, *Energy Environ. Sci.*,2013, **6**, 1388-1414.
10. H. Du, X. Xie, Q. Zhu, L. Lin, Y. F. Jiang, Z. K. Yang, X. Zhou and A. W. Xu, *Nanoscale*., 2015, **7**, 5752-5759.
11. T. Kavithaa, A. I. Gopalanb, K. P. Leeb and S. Y. Park, *Carbon*., 2012, **50**, 2994-3000.
12. J. Mao, T. Y. Peng, X. H. Zhang, K. Li, L. Q. Ye and L. Zan, *Catal. Sci. Technol.*, 2013, **3**, 1253-1260.
13. J. L. Lin, Z. M. Pan and X. C. Wang, *ACS Sustainable Chem. Eng.*, 2014, **2**, 353-358.
14. A. Fujiashima and K. Honda, *Nature*., 1972, **238**, 37-38.
15. L. Ge, C. C. Han, X. L. Xiao and L. L. Guo, *Appl. Catal., B*, 2013, **142-143**, 414-422.
16. F. Fina, S. K. Callear, G. M. Carins, and J. T. S. Irvine, Chem. *Mater.*, 2015, **27**, 2612-2618.
17. H. Xu, J. Yan, Y. G. Xu, Y. H. Song, H. M. Li, J. X. Xia, C. J. Huang and H. L. Wan, *Appl. Catal., B*, 2013, **129**,182-193.
18. X. C. Wang, K. Maeda, A. Thomas, K. Takanabe, G. Xin, J. M. Carlsson, K. A. Domen and M. Antonietti, *Nat. Mater.*, 2009, **8**,76-80.
19. A. Thomas, A. Fischer, F. Goettmann, M. Antonietti, J. Müller, R. Schlögl and J. M. Carlsson, *J. Mater. Chem.*, 2008, **18**, 4893-4908.
20. J. J. Zhu, P. Xiao, H. L. Li and S. A. C. Carabineiro, *ACS Appl. Mater. Interfaces*, 2014, **6**, 16449-16465.
21. G. P. Dong, Y. H. Zhang, Q. W. Pan and J. R. Qiu, *J. Photochem. Photobiol., C*, 2014, **20**,33-50.
22. Y. J. Zhang, T. Mori, L Niu and J. H. Ye, *Energy Environ. Sci.*, 2011, **4**, 4517.
23. Y. M. He, J. Cai, T. T. Li, Y. Wu,Y. M. Yi, M. F. Luo and L. H. Zhao, *Ind. Eng. Chem. Res.*, 2012, **51**, 14729-14737.
24. S. Chu, Y. Wang, Y. Guo, J. Y. Feng, C. C. Wang, W. J. Luo, X. X. Fan and Z. G. Zou, *ACS Catal.*, 2013, **3**, 912-919.
25. X. J. Bai,R. L. Zong, C. X. Li, D. Liu, Y. F. Liu and Y. F. Zhu, *Appl. Catal., B*, 2014, **147**, 82-91.
26. J. Liu, Y. M. Yang, N. Y. Liu, Y. Liu, H. Huang and Z. H. Kang, *Green Chem.*, 2014, **16**,

4559-4565.
27. J. G. Yu, K. Wang, W. Xiao and B. Cheng, *Phys. Chem. Chem. Phys.*, 2014, **16**, 11492-11501.
28. C. C. Han, L. E. Wu, L. Ge, Y. J. Li and Z. Zhao, *Carbon*, 2015, **92**, 31-40.
29. X. J. Bai, L. Wang, R. L. Zong and Y. F. Zhu, *J. Phys. Chem. C*, 2013, **117**, 9952-9961.
30. Y. J. Zhou, L. X. Zhang, J. J. Liu, X. Q. Fan, B. Z. Wang, M. Wang, W. C. Ren, J. Wang, M. L. Lia and J. L. Shi, *J. Mater. Chem. A*, 2015, **3**, 3862-3867.
31. G. Chen and S. P. Gao, *Chin. Phys. B*, 2012, **21**, 107101.
32. X. J. She, H. Xu, H. F. Wang, J. X. Xia, Y. H. Song, J. Yan, Y. G. Xu, Q. Zhang, D. L. Du and H. M. Li, *Dalton Trans.*, 2015, **44**, 7021-7031.
33. Y. Hou, F. Zuo, A. P. Dagg, J. K. Liu and P. Y. Feng, *Adv. Mater.*, 2014, **26**, 5043-5049.
34. L. Xu, X. J. Xia, H. Xu, S. Yin, K. Wang, L. Y. Huang, L. G. Wang and H. M. Li, *J. Power Sources*, 2014, **245**, 866-874.
35. C. C. Han, L. Ge, C. F. Chen, Y. J. Li, X. L. Xiao,Y. N. Zhang and L. L. Guo, *Appl. Catal., B*, 2014, **147**, 546-553.
36. S. X. Min and G. X. Lu, *J. Phys. Chem. C*, 2012, **116**, 19644-19652.
37. H. Xu, J. Yan, X. J. She, L. Xu, J. X. Xia, Y. G. Xu, Y. H. Song, L. Y. Huang and H. M. Li, *Nanoscale*., 2014, **6**, 1406-1415.
38. J. G. Yu, H. G. Yu, B. Cheng, X. J. Zhao, J. C.Yu and W. K. Ho, *J. Phys. Chem. B*, 2003, **107**, 13871-13879.
39. M. Hamadanian, A. Reisi-Vanani and A. Majedi, *Appl. Surf. Sci.*, 2010, **256**, 1837-1844.
40. R. Mehdi and T. Nasrin, *Mater. Chem. Phys.*, 2011, **129**, 249-255.
41. Y. L. Chen, D. Z. Li, X. C. Wang, X. X. Wang and X. Z. Fu, *Chem. Commun.*, 2004, **20**, 2304-2305.
42. B. S. Liu, X. J. Zhao, Q. N. Zhao, C. L. Li and X. He, *Mater. Chem. Phys.*, 2005, **1**, 53-63.
43. W. W. Tu, J. P. Lei, P. Wang and H. X. Ju, *Chem. Eur. J.*, 2011, **17**, 9440-9447.
44. L. Xu, J. X. Xia, H. Xu, J. Qian, J. Yan, L. G. Wang, K. Wang and H. M. Li, *Analyst*., 2013,**138**, 6721-6726.
45. V. W. Lau, M. B. Mesch, V. Duppel, V. Blum, J. Senker and B. V. Lotsch, *J. Am. Chem. Soc.*, 2015, **137**, 1064-1072.
46. A. Thomas, A. Fischer, F. Goettmann, M. Antonietti, J. O. Muller, R. Schlogl and J. M. Carlsson, *J. Mater. Chem.*, 2008, **18**, 4893-4908.
47. Y. G. Li, J. A. Zhang, Q. S. Wang, Y. X. Jin, D. H. Huang, Q. L. Cui and G. T. Zou, *J. Phys. Chem. B*, 2010, **114**, 9429-9434.
48. Q. J. Xiang, J. G. Yu and M. Jaroniec, *J. Phys. Chem. C*, 2011, **115**, 7355-7363.
49. A. B. Jorge, D. J. DMartin, M. T. S. Dhanoa, A. S. Rahman, N. Makwana, J. Tang, A. Sella, F. Corà, S. Firth and J. A. Darr, *J. Phys. Chem. C*, 2013, **117**, 7178-7185.
50. Y. Zheng, J. Liu, J. Liang, M. Jaroniec and S. Z. Qiao, *Energy Environ. Sci.*, 2012, **5**, 6717-6731.
51. X. J. She, H. Xu, Y. G. Xu, J. Yan, J. X. Xia, L. Xu, Y. H. Song, Y. Jiang, Q. Zhang and H. M. Li, *J. Mater. Chem. A*, 2014, **2**, 2563-2570.
52. F. Dong, Z. W. Zhao, T. Xiong, Z. L. Ni, W. D. Zhang, Y. J. Sun, and W. K. Ho, *ACS Appl. Mater. Interfaces*, 2013, **5**, 11392-11401.
53. J. H. Li, B. Shen, Z. H. Hong, B. Z. Lin, B. F. Gao and Y. L. Chen, *Chem. Commun.*, 2012, **48**, 12017-12019.

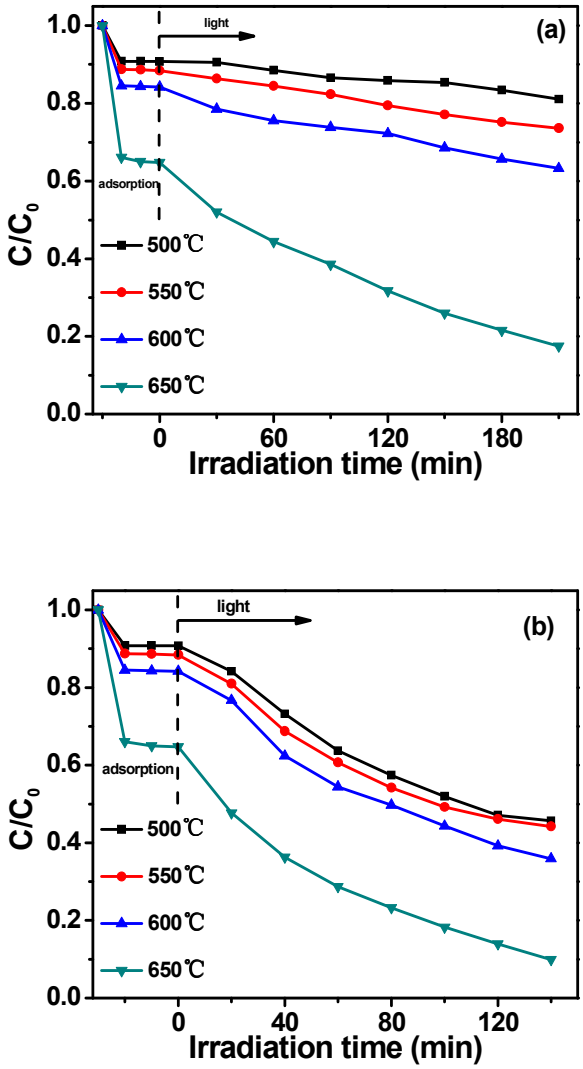

Fig. 1 (a) Photocatalytic activity of g-C_3N_4 prepared at different temperatures for the degradation of MB under visible light irradiation; (b) Photocatalytic activity of g-C_3N_4 prepared at different temperatures for the degradation of MB under UV-light irradiation.

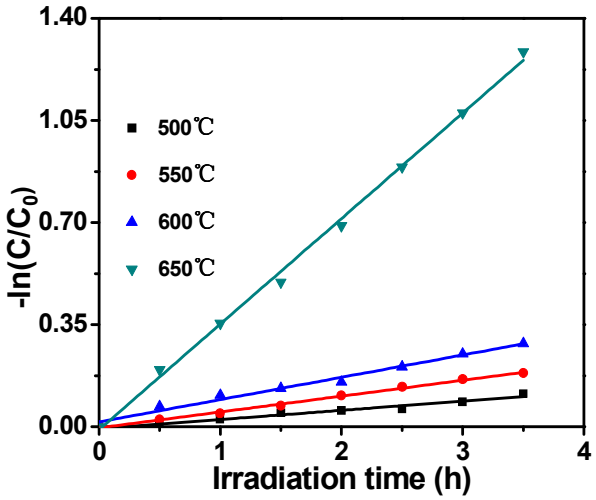

Fig. 2 Kinetic fit for the degradation of MB under visible light irradiation with g-C_3N_4 prepared at different temperatures.

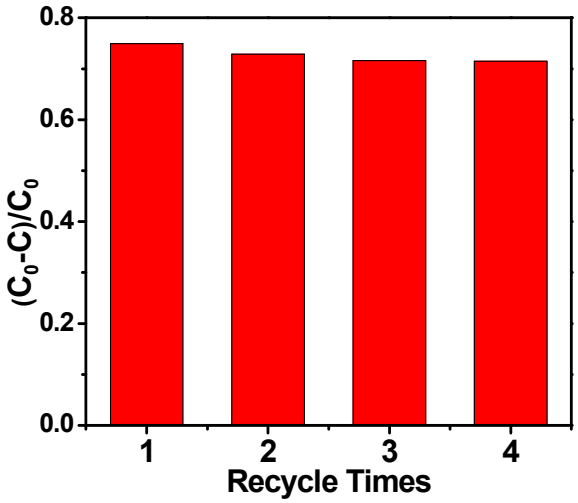

Fig. 3 Cycling runs for the photocatalytic degradation of MB in the presence of g-C_3N_4 prepared at 650°C under visible light irradiation.

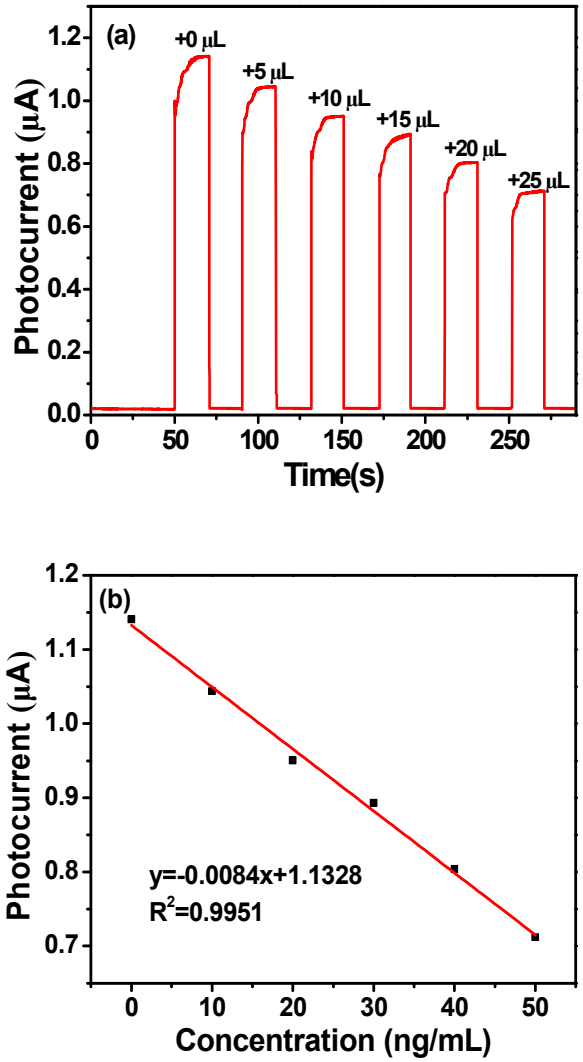

Fig. 4 (a) Photocurrent intensity of ITO/g-C_3N_4 prepared at 650°C in the present of 0, 5, 10, 15, 20, 25 μL MB (10 mg/L) at -0.2 V with visible light irradiation ([Na_2SO_4] = 0.1 M) and its linear calibration curve.

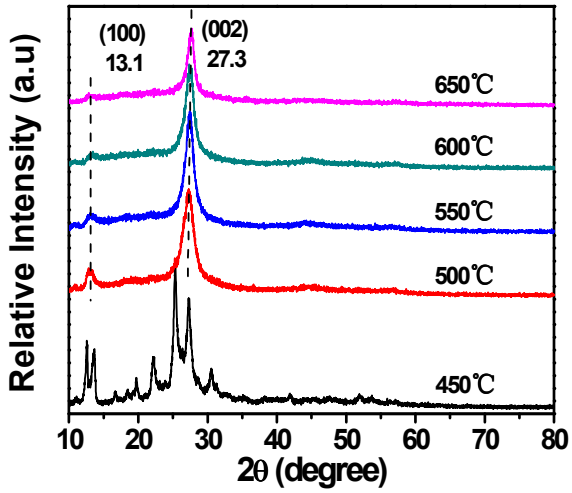

Fig. 5 X-ray patterns of g-C_3N_4 prepared at different temperatures.

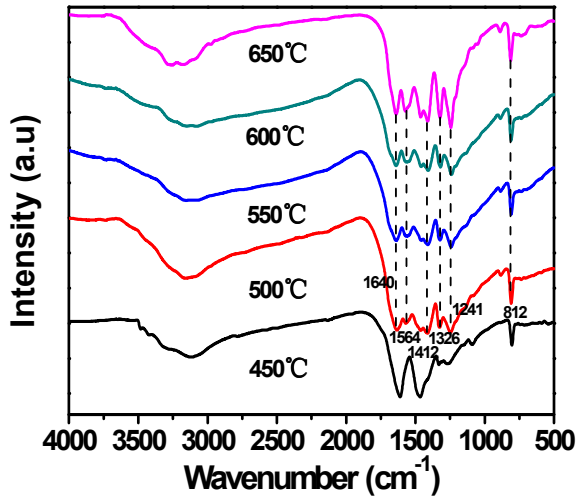

Fig. 6 FT-IR patterns of g-C_3N_4 prepared at different temperatures.

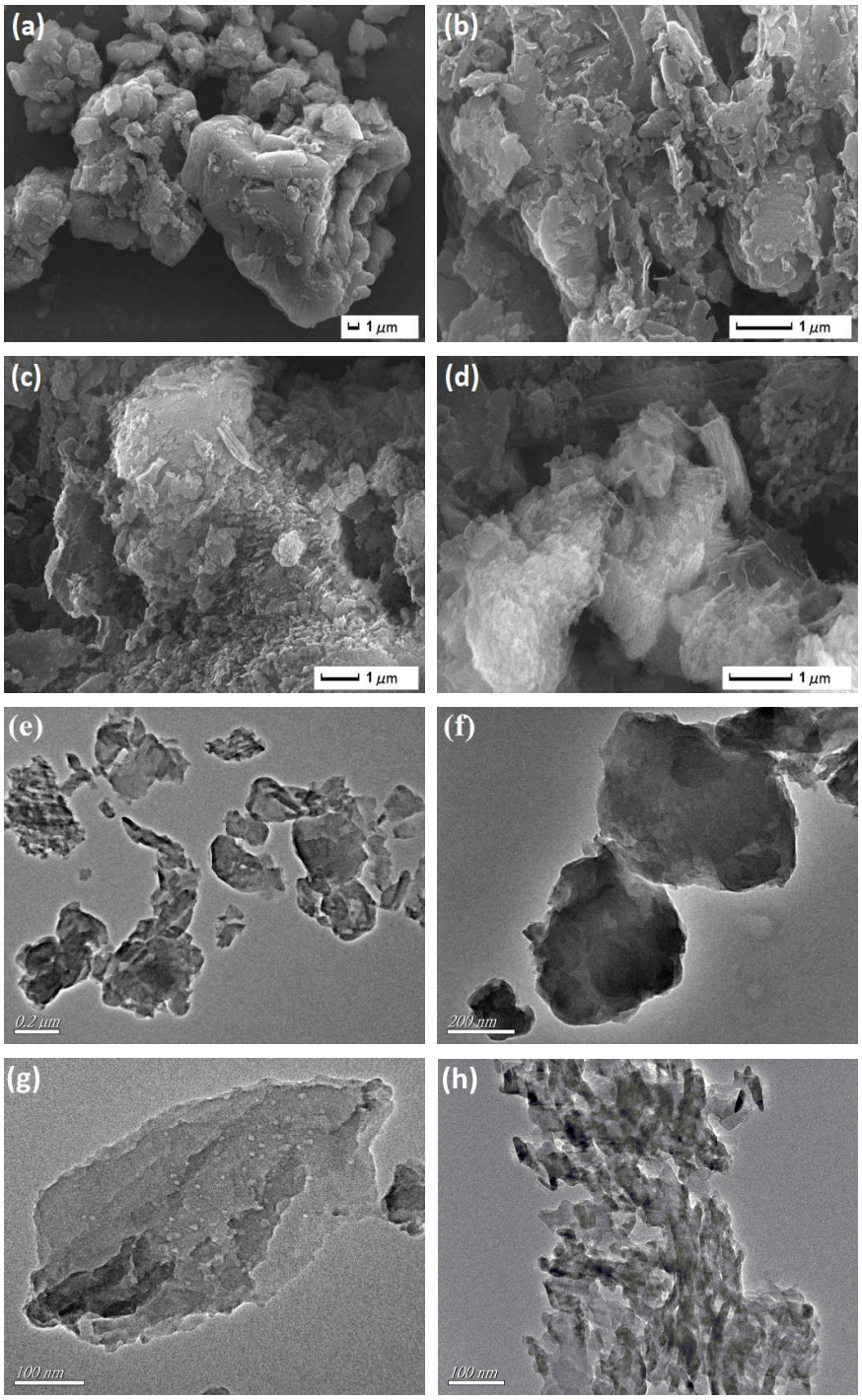

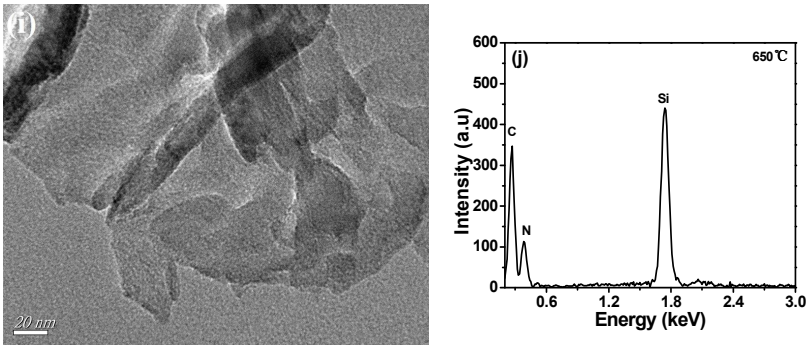

Fig. 7 SEM images of g-C_3N_4 prepared at different temperatures (a) 500°C, (b) 550°C, (c) 600°C (d) 650°C; TEM images of g-C_3N_4 prepared at different temperatures (e) 500°C, (f) 550°C, (g) 600°C, (h) 650°C (i) high-magnification TEM image of g-C_3N_4 prepared at 650°C and (j) EDS analysis of g-C_3N_4 prepared at 650°C.

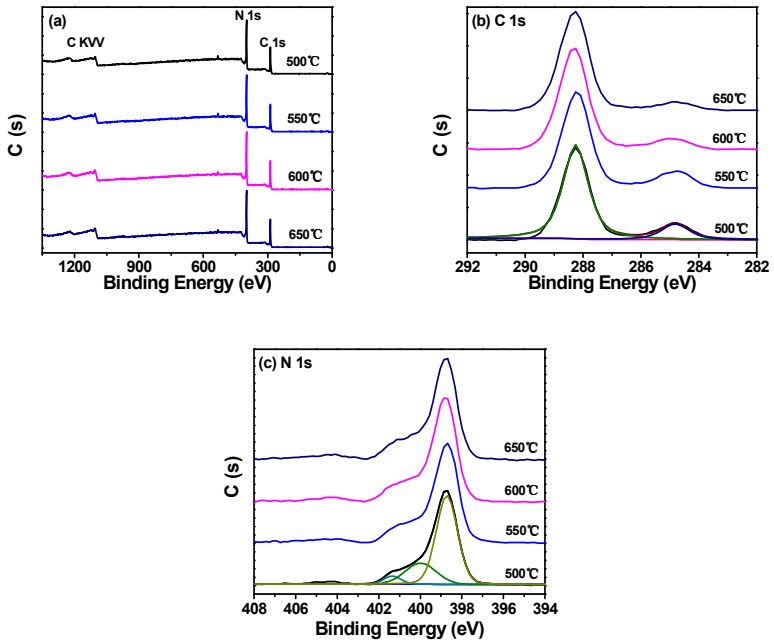

Fig. 8 XPS spectra of g-C_3N_4 prepared at different temperatures (a) survey, (b) C 1s, (c) N 1s.

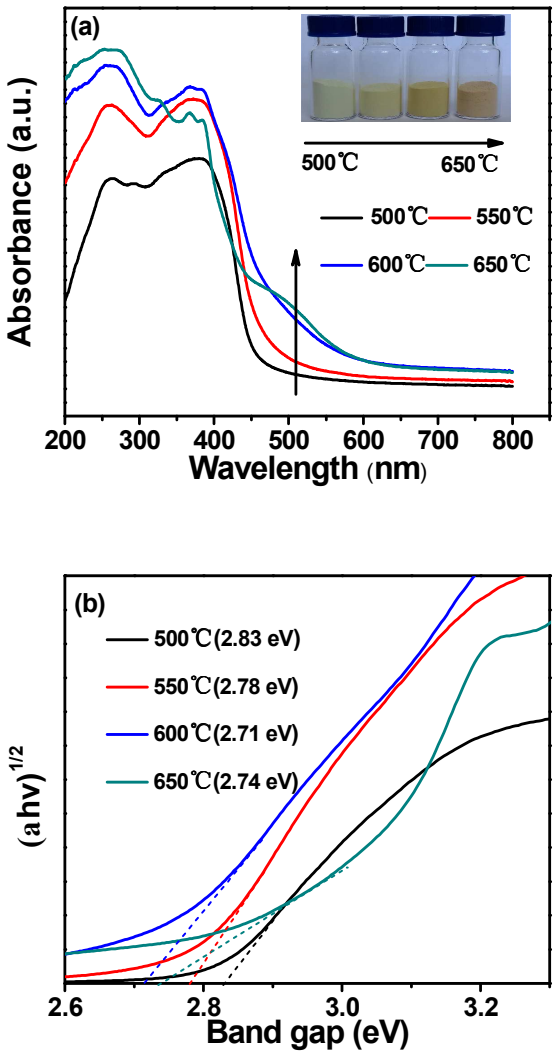

Fig. 9 (a) UV-vis diffuse reflectance spectra and (b) Estimated band gaps of g-C_3N_4 prepared at different temperatures.

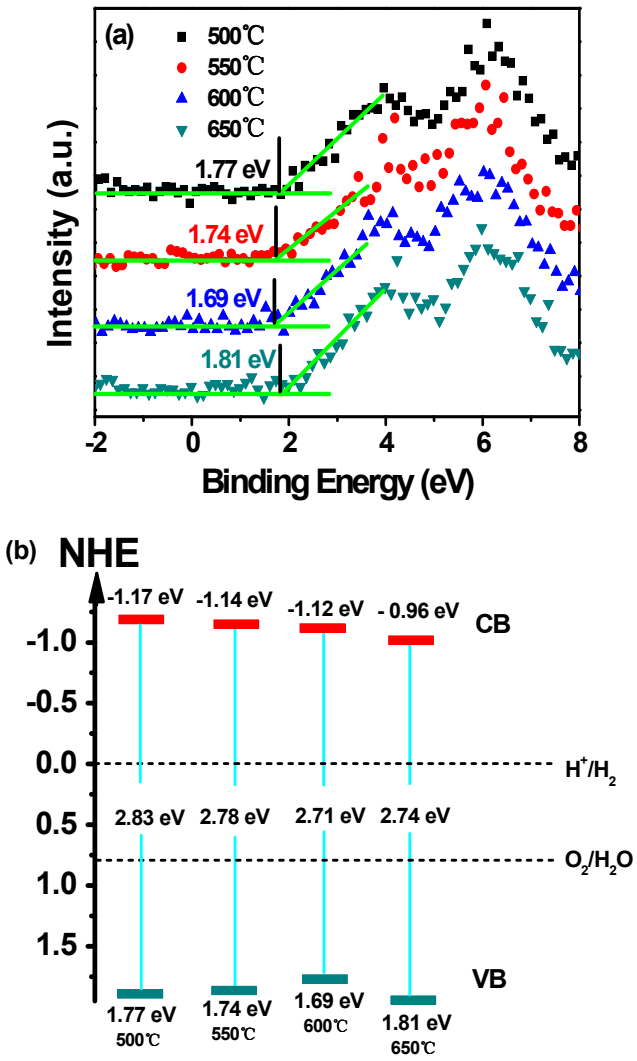

Fig. 10 (a) VB XPS spectra of g-C_3N_4 prepared at different temperatures and (b) Schematic illustration of the band structures of g-C_3N_4 prepared at different temperatures.

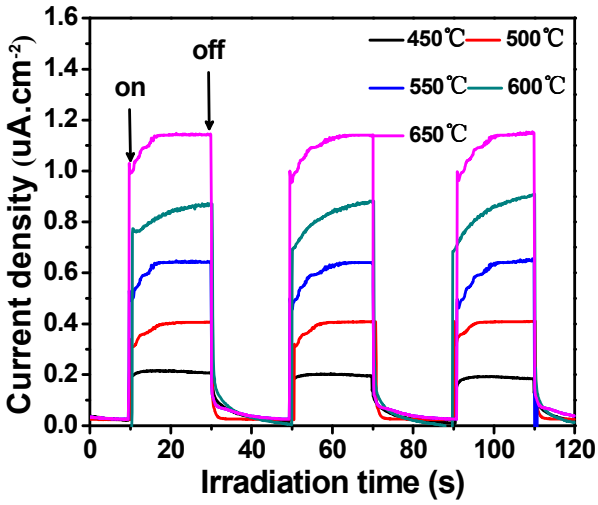

Fig. 11 Photocurrent responses of g-C_3N_4 prepared at different temperatures under visible light irradiation ([Na_2SO_4] = 0.1 M).

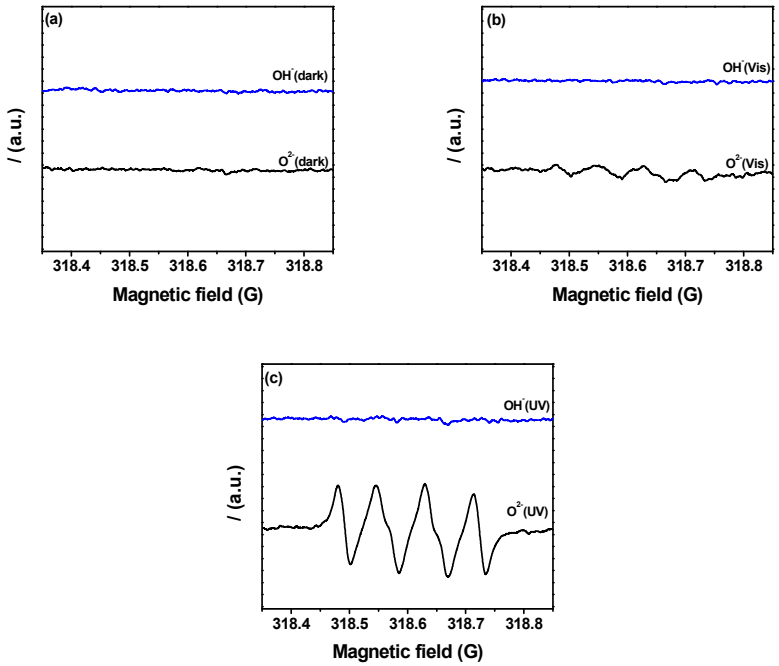

Fig. 12 ESR spectra of g-C_3N_4 prepared at 650°C (a) in the dark; (b) after visible light irradiation and (c) under UV-light irradiation.

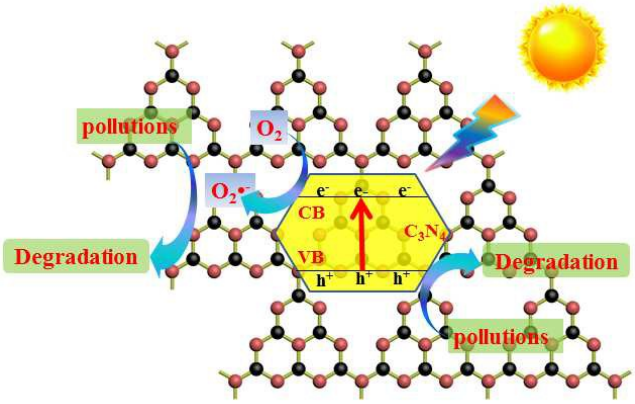

Fig. 13 Visible/UV Photocatalytic mechanism diagram of g-C_3N_4.

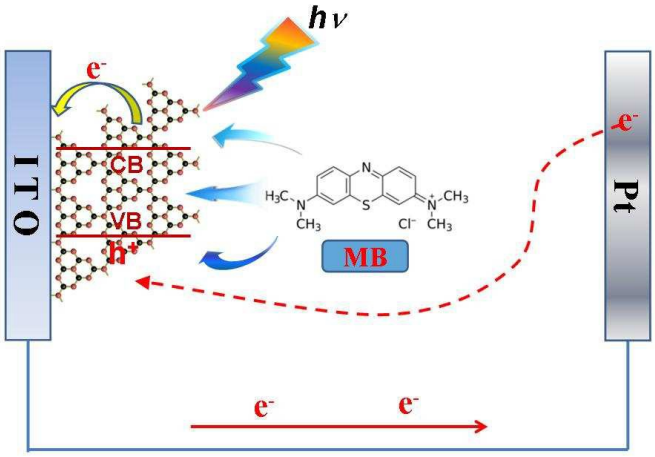

Fig. 14 Schematic illustration of possible photoelectrochemical mechanism for detection of MB.

Synthesis of g-C_3N_4 prepared at different temperatures for superior visible/UV photocatalytic performance and photoelectrochemical sensing of MB solution

Zhao Mo, Xiaojie She, Yeping Li, Liang Liu, Liying Huang, Zhigang Chen, Qi Zhang, Hui Xu*, Huaming Li*

School of Chemistry and Chemical Engineering, *Institute for Energy Research, Jiangsu University, Zhenjiang 212013, P. R. China*

***Corresponding author:** Tel.:+86-511-88791800; Fax: +86-511-88791708;
E-mail address: xh@ujs.edu.cn, lihm@ujs.edu.cn

The visible light absorption of g-C_3N_4 was extended through controlling the synthesis temperature, and thus enhanced visible/UV photocatalytic activity. Moreover, g-C_3N_4 can also be used as a photoelectrochemical sensor.